

Prospects for detecting gravitational waves at 5 Hz with ground-based detectors

Hang Yu,^{*} Denis Martynov,[†] Salvatore Vitale, Matthew Evans, and David Shoemaker
LIGO, Massachusetts Institute of Technology, Cambridge, Massachusetts 02139, USA

Bryan Barr, Giles Hammond, Stefan Hild, James Hough, Sabina Huttner, Sheila Rowan, and Borja Sorazu
SUPA, University of Glasgow, Glasgow G12 8QQ, United Kingdom

Ludovico Carbone, Andreas Freise, and Conor Mow-Lowry
*School of Physics and Astronomy and Institute of Gravitational Wave Astronomy,
University of Birmingham, Edgbaston, Birmingham B15 2TT, United Kingdom*

Katherine L. Dooley
The University of Mississippi, University, Mississippi 38677, USA

Paul Fulda
NASA Goddard Space Flight Center, Greenbelt, Maryland 20771, USA

Hartmut Grote
Max-Planck Institut für Gravitationsphysik und Leibniz Universität Hannover, D-30167 Hannover, Germany

Daniel Sigg
LIGO Hanford Observatory, Richland, Washington 99352, USA

(Dated: December 18, 2017)

We propose an upgrade of Advanced LIGO (aLIGO), named LIGO-LF, that focuses on improving the sensitivity in the 5-30 Hz low-frequency band, and we explore the upgrade's astrophysical applications. We present a comprehensive study of the detector's technical noises, and show that with the new technologies such as interferometrically-sensed seismometers and balanced-homodyne readout, LIGO-LF can reach the fundamental limits set by quantum and thermal noises down to 5 Hz. These technologies are also directly applicable to the future generation of detectors. LIGO-LF can observe a rich array of astrophysical sources such as binary black holes with total mass up to $2000 M_{\odot}$. The horizon distance of a single LIGO-LF detector will be $z \simeq 6$, greatly exceeding aLIGO's reach. Additionally, for a given source the chirp mass and total mass can be constrained 2 times better, and the effective spin 3-5 times better, than aLIGO. The total number of detected merging black holes will increase by a factor of 16 compared with aLIGO. Meanwhile, LIGO-LF will also significantly enhance the probability of detecting other astrophysical phenomena including the gravitational memory effects and the neutron star r-mode resonances.

Introduction.— The detections of gravitational waves (GWs) from coalescing binary black holes (BHs) [1–3] by aLIGO [4] and Advanced Virgo (aVirgo) [5] heralded the era of GW astrophysics. While the detections have shown that there is an abundant population of BHs in the mass range from 7 to $70 M_{\odot}$ within redshift $z \lesssim 0.2$, detecting binaries that are more massive and further away is challenging. Since the merger frequency decreases as the total mass of the binary increases, systems more massive than a few hundred solar mass will no longer lie in the most sensitive band of aLIGO. The intermediate-mass black holes (IMBHs) with masses $\sim 10^2 - 10^4 M_{\odot}$ [6] are such examples. Even after aLIGO reaches its design sensitivity, only relatively low mass IMBHs can be detected [7–10]. At the same time, for sources further away, the GW signal seen by the detectors is also shifted to lower frequencies due to the cosmological redshift [11]. Therefore, improving the low-frequency sensitivity of GW detectors

plays a crucial role in extending both the mass and spatial range of detectability.

In this Letter we propose an upgrade to aLIGO (and its evolution, A+ [12]) that enables a significant enhancement in sensitivity in the 5-30 Hz band, and maintains high frequency performance. This new design, dubbed “LIGO-LF”, can be achieved in the current infrastructure, and be implemented on a timescale of 10 years. In addition to LIGO-LF's merits in astrophysics, the design and commissioning of it will also shed light on both later upgrades like the Voyager [13] and future generations of GW detectors like the Einstein Telescope [14, 15] and the Cosmic Explorer [16].

LIGO-LF design. – Some of the technical noises in aLIGO are currently more than an order of magnitude above the instrument's fundamental limits at 10 Hz [17–19]. In this section we describe the solutions we propose to reach the LIGO-LF sensitivity shown in FIG. 1.

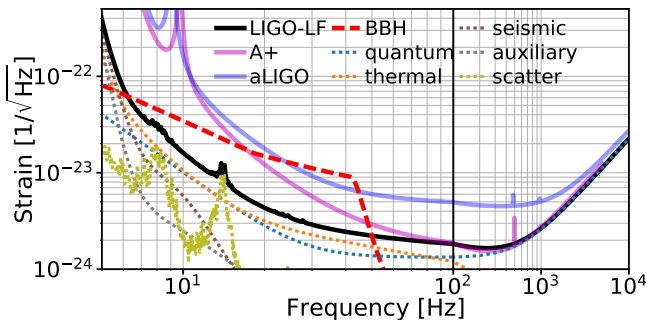


FIG. 1. Proposed sensitivity curve for LIGO-LF (solid-black), with a noise budget including contributions from both fundamental noises and technical noises (dashed lines). Also shown in the dotted-red curve is the spectrum of a $200 M_{\odot} - 200 M_{\odot}$ binary BH merger (in the detector frame) at 10Gpc with optimal orientation as the main astrophysical target of the upgrade. The LIGO-LF sensitivity to such systems is greatly enhanced relative to aLIGO (solid-blue) and A+ (solid-magenta).

During the first detections of GWs, a low-frequency cutoff was set to 20 Hz [1–3, 20]. Data at lower frequencies were not used because time-dependent coupling of the control noise from the auxiliary degrees of freedom limits the current aLIGO sensitivity. The first element of the upgrade proposed for LIGO-LF reduces the angular control noise.

Angular motion of the aLIGO optics is actively stabilized using wave-front sensors with a typical sensitivity of 5×10^{-15} rad/ $\sqrt{\text{Hz}}$ [18, 21]. The bandwidth of the arm cavity angular loops is set to 3 Hz to reduce the seismically induced motion of the test masses down to a few nrad rms. However, the control noise disturbs the test masses above 5 Hz and couples to the GW readout significantly via the beam miscentering on the mirrors. To reduce this noise, we propose to further suppress the motion of the optical benches so that the bandwidth of the angular loops can be lowered.

Despite the sophistication of the LIGO seismic isolation systems [22–24], it does not significantly reduce the ground motion at microseism frequencies. This is due to the tilt-to-horizontal coupling [25–27], which causes the horizontal sensitivity of the aLIGO inertial sensors to grow very unfavorably (as $1/f^4$) at low frequencies as shown in FIG. 2. In order to reduce the bandwidth of the angular controls down to around 1 Hz, sensitivity of the tilt sensor should be 10^{-10} rad/ $\sqrt{\text{Hz}}$ in the frequency range 10 mHz to 0.5 Hz. The corresponding horizontal sensitivity is shown in FIG. 2. Above 1 Hz we require an improved sensitivity to reduce the direct coupling of the ground motion to the GW channel (see the Supplemental Material for a breakdown of the angular control noise).

There are two current approaches to reach the required sensitivity of the inertial seismic sensors. The first one is to actively stabilize tilt motion using 1D tiltmeters.

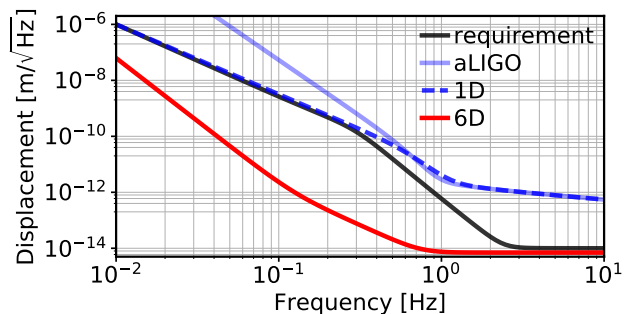


FIG. 2. Inertial sensor noise for aLIGO (blue), required sensor noise for LIGO-LF (black). A 1D tiltmeter can be used to improve aLIGO sensor noise below 0.5 Hz (blue-dashed). A novel 6D optical seismometer can surpass the requirement (red).

These rotation sensors, custom built at the University of Washington, have an improved tilt sensitivity compared to commercial ones [28, 29]. Using these tiltmeters, the required sensitivity below 0.5 Hz can be achieved. The second approach uses an optical 6D seismometer proposed in [30]. In the core of this instrument is an inertial mass whose position is monitored relative to the optical bench using interferometric readout. The mass is suspended using fused silica fibers and the whole assembly is quasimonolithic [31]. FIG. 2 shows that the design performance of the 6D optical seismometer satisfies the requirement in the entire frequency band.

Another factor limiting the minimum bandwidth of aLIGO is the need of suppressing an angular instability induced by radiation-pressure [32, 33]. We propose to increase the LIGO-LF test masses from 40 kg to 200 kg because heavier masses are less subject to the effects of radiation pressure.

The next technique required for LIGO-LF is balanced-homodyne readout [34]. This scheme is crucial to reduce the coupling of the longitudinal motion of the signal recycling cavity to the GW channel. The coupling is mediated by radiation pressure [35] and originates from the fact that the two arms are intentionally detuned to enable DC readout [36]. In aLIGO, this noise is one of the dominant noise sources in the 10-50 Hz band [18]. Nevertheless, it can be essentially eliminated in LIGO-LF, because balanced-homodyne readout eliminates the requirement for an intentional detuning of the arms. The scheme also makes the laser intensity noise insignificant above 5 Hz.

The next problem we consider is suspension damping. High-quality-factor resonances are damped using shadow sensors [37] with a sensing noise of 2×10^{-10} m/ $\sqrt{\text{Hz}}$. The damping control noise is a significant factor for aLIGO performance. A global control scheme has been proposed [38] to reduce the direct coupling of longitudinal damping noise to the GW channel. The shadow sensor

noise, however, enters the auxiliary loops and couples to the GW channel. This calls for an improvement of the sensor noise by a factor of 100. Interferometric sensors [39] are promising candidates and can significantly surpass the requirement.

Once technical and environmental noises are suppressed in the frequency range 5-30 Hz, LIGO-LF sensitivity will be limited by quantum and thermal noises. Our strategy to improve the fundamental limits is similar to the Strawman Team Red design [40].

Quantum noise [41–43] manifests both as sensor shot noise, and as displacement noise by exerting quantum radiation pressure (QRP) forces on the test masses. LIGO-LF will operate under the “resonant-sideband extraction” configuration [44] with the same amount of power circulating in the arms as aLIGO. A signal recycling mirror (SRM) power transmissivity of 0.25 is chosen to optimize the broadband sensitivity. The quantum noise can be reduced with squeezed light [45–47]. Here we assume a frequency-dependent squeezing [48–50] that provides 3 dB reduction of the QRP noise and 6 dB of the shot noise. The QRP is further suppressed as the test masses are increased from 40 kg to 200 kg.

Thermal noise is mainly due to the Brownian motion [51] in the suspension and the optical coatings. Below 20 Hz, suspension thermal noise dominates and is mildly suppressed by the heavier test masses [31, 52, 53]. The length of the last suspension stage is doubled to 1.2 m to fully utilize the capacity of aLIGO’s vacuum enclosure, which provides extra filtering and dilution of the effective mechanical loss [54]. Meanwhile, the loss can be lowered with more sophisticated surface treatments [55]. To reduce the noise from the upper stages, the penultimate masses of LIGO-LF are also suspended with fused silica fibers. Overall, a factor of 5 improvement over the aLIGO baseline is possible. The vertical component couples weakly and its resonance can be shifted down to 4.3 Hz by a combination of increasing both the length of the suspension and the tension inside the fiber (see the Supplemental Material for a detailed description of LIGO-LF suspension).

The coating thermal noise [43, 56–59] dominates the sensitivity in the band from a few ten to a few hundred Hz. The larger test masses and better seismic isolation open up the possibility of increasing spot sizes by 50% while keeping the alignment manageable. Furthermore, a factor of 2 improvement in material loss angle is expected by the time of LIGO-LF [60].

Further sensitivity improvement below 30 Hz is limited by the gravity gradient noise and scattered light noise. Fluctuations of local gravity fields around the test masses [61–63] couple to the GW channel as force noise. It can be partially suppressed using offline regression techniques [64]. In our calculation, a factor of 10 cancellation is assumed [16]. The residual gravity gradient noise is combined with the residual seismic motion in

FIG. 1 under the label ‘seismic’.

Scattering in the arm tubes leads to a critical noise contribution below 30 Hz [17, 65, 66]. A small amount of light can scatter off the test masses due to surface imperfections, hit the baffles along the beam tubes, and finally recombine with the main beam. At low frequencies, the amplitude quadrature of the scattered light dominates the coupling, with a coefficient

$$Z_{\text{scatter}} \simeq 8.2 \times 10^{-13} \left(\frac{20\text{Hz}}{f} \right)^2 \left(\frac{200\text{kg}}{m_{\text{tm}}} \right) \frac{\text{m}}{\text{m}}. \quad (1)$$

The coupling becomes a constant above 20 Hz. As the relative displacement between the test mass and the beam tube is on the order of the laser wavelength ($1 \mu\text{m}$), the scattered light noise coupling can thus be nonlinear. This nonlinearity leads to up-conversion (known as “fringe-wrapping” [18, 67]) of the baffle motion below 0.4 Hz up to 5 Hz. In FIG. 1 we present a scattering noise curve estimated from typical ground motion at the LIGO sites with an anticipated 50% improvement in the mirror surface quality relative to aLIGO. For rare cases where the ground motion is severe, an up-conversion shelf can form [17] and limit the low frequency sensitivity.

The anti-reflecting surfaces along the optical path create another kind of scattering noise. To suppress this noise, baffles should be constructed in the vertex of the interferometer to block at least 99.9% of the total stray light (see the Supplemental Material for a breakdown of the total scattering noise).

Parameter estimation of coalescing IMBHs.— With the LIGO-LF upgrade, both the number of detections and the maximum detectable mass are larger than with aLIGO and A+, as illustrated in the left panel of FIG. 3. Here we plot the LIGO-LF horizon and range [68] as a function of the total mass. The system is assumed to be non-spinning and to have equal masses. A single LIGO-LF could detect IMBHs to cosmological distances ($z \simeq 6$), whereas a network of 4 detectors would observe to $z \sim 10$, potentially accessing the first generation of stellar BHs [69].

Moreover, for a given system, LIGO-LF enables a significantly more accurate parameter estimation than aLIGO. This is due to two facts: more total signal-to-noise ratio (SNR) is accumulated in LIGO-LF than in aLIGO, and the SNR starts to accumulate at lower frequencies (right panel of FIG. 3). Thus, if aLIGO can only measure the late merger-ringdown phase of an IMBH coalescence, with LIGO-LF we would be able to access the inspiral phase as well. This allows for a more precise estimation of the component masses and spins, essential for characterizing the IMBHs.

To quantify these improvements, we analyze simulated IMBH signals in mock interferometric data. Since the sensitivity of A+ and aLIGO are similar below 20 Hz (where IMBHs’ inspirals would live) we consider the com-

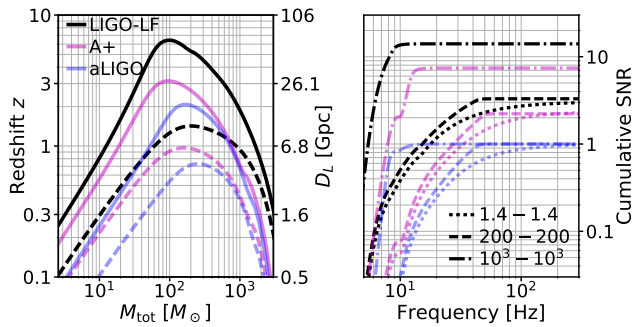


FIG. 3. Left: The horizon (solid lines) and range (dashed lines) for LIGO-LF (blue), A+ (magenta), and aLIGO (black). The mass is in the source frame. LIGO-LF may reach a cosmological redshift $z \simeq 6$. Right: the cumulative SNR for different binaries. For a given system, the total SNR seen in aLIGO is normalized to 1. Not only more total SNR can be recovered in LIGO-LF than in aLIGO, the SNR also starts to accumulate at lower frequencies, increasing the number of useful cycles [70].

parison between LIGO-LF and aLIGO. The IMBH signals are generated with the `IMRphenomPv2` waveform [71]. We consider 5 total mass bins from $100 M_\odot$ to $2000 M_\odot$. For each source, we realize 3 spin configurations: no-spin ($\chi_{\text{eff}} = \chi_p = 0$), precessing spins with positive χ_{eff} ($\chi_{\text{eff}} = 0.5$, $\chi_p = 0.6$), and precessing spins with negative χ_{eff} ($\chi_{\text{eff}} = -0.5$, $\chi_p = 0.6$). Here χ_{eff} is the mass-weighted sum of component spins along the orbital angular momentum [72, 73], whereas χ_p captures the precessing component [74]. The effect of mass ratio has been studied in REF. [9] so we focus on the equal mass case. The waveforms are added to mock noise of a detector network formed by the Livingston site (L), the Hanford site (H), LIGO-India (I), and aVirgo (V). For the LHI network, we consider both the LIGO-LF and aLIGO design sensitivity; for V, we fix it at its design sensitivity [5] so that we can focus on the improvements due to LIGO-LF. KAGRA [75] is not included as it is less sensitive to IMBHs compared to other detectors. For each source, the inclination is fixed to 30° and the distance is chosen such that the network SNR is 16 when the aLIGO instruments are used. We then use the `LALInference` [76] to get posterior distributions of the IMBH parameters. The analysis is performed from a lower frequency of 4.5 Hz (5.5 Hz) for LIGO-LF (aLIGO). In this section, we refer to the detector frame and we denote it with a superscript (d).

In FIG. 4 we plot the 90% credible intervals of the posterior distributions of the chirp mass $\mathcal{M}_c^{(d)}$, total mass $M_{\text{tot}}^{(d)}$, and χ_{eff} . For the masses, we present the results for the non-spinning case. Fractionally, $M_{\text{tot}}^{(d)}$ is better constrained than $\mathcal{M}_c^{(d)}$ for both LIGO-LF and aLIGO, because for systems this massive, the merger-ringdown phase dominates the SNR (cf., the right panel of FIG. 3; also [9]). When spins are included, an aligned (anti-

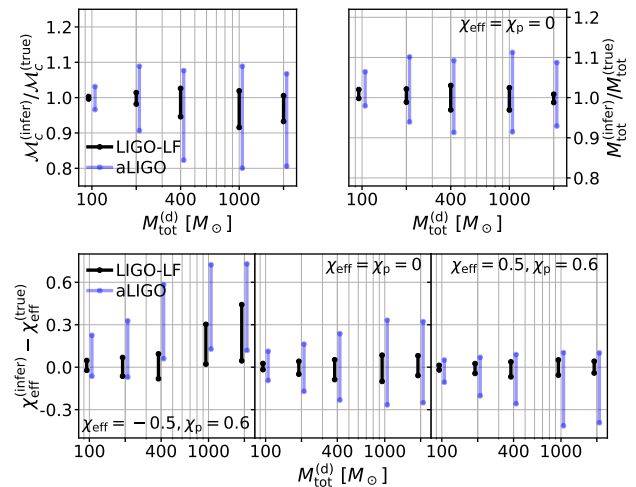


FIG. 4. The 90% credible intervals of the detector frame chirp mass $\mathcal{M}_c^{(d)}$ (top-left panel), total mass $M_{\text{tot}}^{(d)}$ (the top-right panel), and effective spin χ_{eff} (bottom panels) are all significantly smaller for LIGO-LF (black) than for aLIGO (blue). LIGO-LF also reduces biases, especially for $\mathcal{M}_c^{(d)}$ and χ_{eff} when the spin is anti-aligned, as seen in the bottom-left panel.

aligned) spin tends to improve (degrade) the inference accuracy of $\mathcal{M}_c^{(d)}$ because it increases (decreases) the length of the inspiral phase. Similar effects can also be seen in the posterior distributions of χ_{eff} , as illustrated in the bottom panels. The precession term, χ_p , cannot be well constrained even with LIGO-LF.

To convert the detector frame masses shown above to the source frame, the value of inferred redshift is required [11]. The typical statistical error in redshift measured with LIGO-LF is half of that with aLIGO (see the Supplemental Material for the redshift posteriors). Consequently, LIGO-LF enables a factor of 2 improvement in constraining the source frame masses compared to aLIGO. The effective spin χ_{eff} , nonetheless, is unaffected by the redshift and thus LIGO-LF can achieve 3 – 5 times better accuracy than aLIGO, which will be essential for discriminating between different formation scenarios that predict different spin configurations [77].

Other applications– Besides studying the parameters of a single event, examining the population of mergers can also bear valuable fruit in astrophysics and cosmology. We show in FIG. 5 the expected number of coalescing binary BHs LIGO-LF, A+, and aLIGO, can detect per year, respectively. The rate estimation follows REF. [78]. Specifically, we assume the primary BH’s mass, M_1 , yields a distribution $\propto M_1^{-2.35} \exp(-M_1/M_{\text{cap}})$, with the lower end set to $5 M_\odot$ and higher mass cutoff $M_{\text{cap}} = 60 M_\odot$. The secondary’s mass M_2 is assumed to be uniformly distributed between $5 M_\odot$ and M_1 . We adopt a merger rate of $97(1+z)^2 \text{ Gpc}^{-3} \text{ yr}^{-1}$ [79]. It predicts that LIGO-LF can detect ~ 4000 merging BHs per year, which is 16 times that of aLIGO and 2.4 times that of

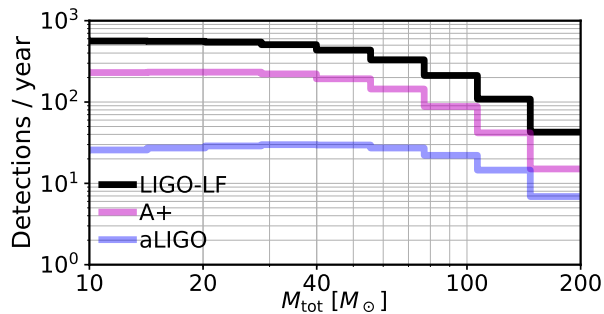


FIG. 5. Expected detections per year of coalescing BH binaries as a function of a system’s total mass. We divide each M_1 and M_2 into 10 logarithmic bins from $5 M_\odot$ to $200 M_\odot$ and marginalize over mass ratio to derive the event rate per total mass bin. LIGO-LF can detect ~ 4000 events per year, 16 times more than the expected number for aLIGO.

A+. The large number of events observed by LIGO-LF may be used to separate binary formation channels that predict different event rates [80, 81], and to constrain the fraction of dark matter in the Universe that is in the form of primordial BHs [78, 82].

Various other astrophysical phenomena may be detected by ground-based GW detectors. Here we consider two more examples: (i) the GW memory effect [83], and (ii) the gravitomagnetic excitation of r-modes in coalescing neutron star (NS) binaries [84]. The results are summarized in FIG. 6. For (i), we adopt the minimal-waveform model [85]. LIGO-LF has a promising probability to detect this effect via event-stacking [86]. We consider (ii) following REF. [84]. Here we focus on the $l = 2, m = 1$ mode. The detectability of r-mode induced phase shift is estimated using a Fisher matrix method (see, e.g., [87]). We find that if the NS spins at rate greater than 35 Hz, LIGO-LF may detect the r-mode resonance from a single event at a distance up to 50 Mpc. Since the phase shift is sensitive to the internal buoyancy, a detection of the r-mode may place constraints on the NS equation of state from physics beyond just the bulk properties of the star [88]. Furthermore, the r-mode provides a measurement of the NS spin, which may help breaking the spin-mass ratio degeneracy [11, 20].

Conclusions.— We proposed the LIGO-LF design to upgrade the current detectors’ low-frequency performance. All advanced technologies required for this update are directly applicable to future generations of detectors. With the LIGO-LF sensitivity, we considered a variety of astrophysical sources, with the focus on the IMBHs. We showed that both the detectability and parameter estimation accuracy were significantly improved.

The authors thank Rainer Weiss, Peter Fritschel, Valery Frolov, Riccardo DeSalvo, Rana Adhikari, and members of the LSC ISC and AIC groups for the valuable discussions and comments. The authors acknowledge the

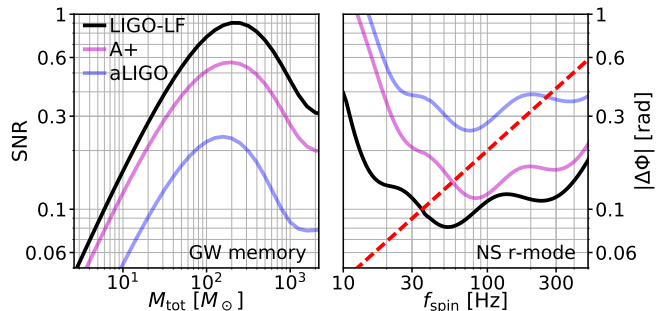


FIG. 6. Examples of astrophysical phenomena that can be searched for with ground-based GW detectors. Right: SNR from the GW memory effect for a source at $z = 0.1$ with inclination angle of 30° as a function of the source frame total mass. Left: The parameter estimation error (solid lines) of the phase shift due to resonant excitation of the NS r-mode as a function of the NS spin frequency, f_{spin} . The corresponding GW frequency of resonance is $4f_{\text{spin}}/3$. The sources are placed face-on at 50 Mpc. Also shown in the red-dashed line is the physical phase shift induced by r-mode resonance. The effect is detectable when this phase shift is greater than the statistical error.

support of the National Science Foundation (NSF) and the Kavli Foundation. LIGO was constructed by the California Institute of Technology and Massachusetts Institute of Technology with funding from the NSF, and operates under cooperative agreement PHY-0757058. Advanced LIGO was built under award PHY-0823459. This material is based upon work supported by the NSF under Grant Number 1608922. HY is supported in part by NASA ATP grant NNX14AB40G (PI Nevin Weinberg). DM is supported by the Kavli Fellowship. LC, CML and AF have been supported by the Science and Technology Facilities Council (STFC).

* hyu45@mit.edu

† denism@mit.edu

- [1] B. P. Abbott, R. Abbott, T. D. Abbott, M. R. Abernathy, F. Acernese, K. Ackley, C. Adams, T. Adams, P. Addesso, R. X. Adhikari, and et al., Physical Review Letters **116**, 061102 (2016), arXiv:1602.03837 [gr-qc].
- [2] B. P. Abbott, R. Abbott, T. D. Abbott, F. Acernese, K. Ackley, C. Adams, T. Adams, P. Addesso, R. X. Adhikari, V. B. Adya, and et al., Physical Review Letters **118**, 221101 (2017), arXiv:1706.01812 [gr-qc].
- [3] B. P. Abbott, R. Abbott, T. D. Abbott, F. Acernese, K. Ackley, C. Adams, T. Adams, P. Addesso, R. X. Adhikari, V. B. Adya, and et al. (LIGO Scientific Collaboration and Virgo Collaboration), Phys. Rev. Lett. **119**, 141101 (2017).
- [4] G. M. Harry and LIGO Scientific Collaboration, Classical and Quantum Gravity **27**, 084006 (2010).
- [5] F. Acernese, M. Agathos, K. Agatsuma, D. Aisa, N. Allemandou, A. Allocca, J. Amarni, P. Astone, G. Balestri,

- G. Ballardini, and et al., *Classical and Quantum Gravity* **32**, 024001 (2015), arXiv:1408.3978 [gr-qc].
- [6] M. Coleman Miller and E. J. M. Colbert, *International Journal of Modern Physics D* **13**, 1 (2004), astro-ph/0308402.
- [7] I. Mandel, D. A. Brown, J. R. Gair, and M. C. Miller, *Astrophys. J.* **681**, 1431-1447 (2008), arXiv:0705.0285.
- [8] P. B. Graff, A. Buonanno, and B. S. Sathyaprakash, *Phys. Rev. D* **92**, 022002 (2015), arXiv:1504.04766 [gr-qc].
- [9] J. Veitch, M. Pürrer, and I. Mandel, *Physical Review Letters* **115**, 141101 (2015), arXiv:1503.05953 [astro-ph.HE].
- [10] B. P. Abbott, R. Abbott, T. D. Abbott, F. Acernese, K. Ackley, C. Adams, T. Adams, P. Addesso, R. X. Adhikari, V. B. Adya, and et al., *Phys. Rev. D* **96**, 022001 (2017), arXiv:1704.04628 [gr-qc].
- [11] C. Cutler and É. E. Flanagan, *Phys. Rev. D* **49**, 2658 (1994), gr-qc/9402014.
- [12] A. Lazzarini, D. Reitze, B. Berger, L. Cadonati, G. Gonzalez, and M. Cavaglia, *What Comes Next for LIGO? Planning for the post-detection era in gravitational-wave detectors and astrophysics*, LIGO (2016), LIGO Document P1600350.
- [13] R. Adhikari, N. Smith, A. Brooks, and et al., *LIGO Voyager Upgrade Concept*, LIGO (2017), LIGO Document T1400226.
- [14] S. Hild, S. Chelkowski, A. Freise, J. Franc, N. Morgado, R. Flaminio, and R. DeSalvo, *Classical and Quantum Gravity* **27**, 015003 (2010), arXiv:0906.2655 [gr-qc].
- [15] B. Sathyaprakash, M. Abernathy, F. Acernese, P. Ajith, B. Allen, P. Amaro-Seoane, N. Andersson, S. Aoudia, K. Arun, P. Astone, and et al., *Classical and Quantum Gravity* **29**, 124013 (2012), arXiv:1206.0331 [gr-qc].
- [16] B. P. Abbott, R. Abbott, T. D. Abbott, M. R. Abernathy, K. Ackley, C. Adams, P. Addesso, R. X. Adhikari, V. B. Adya, C. Affeldt, and et al., *Classical and Quantum Gravity* **34**, 044001 (2017), arXiv:1607.08697 [astro-ph.IM].
- [17] D. V. Martynov, *Lock Acquisition and Sensitivity Analysis of Advanced LIGO Interferometers*, Ph.D. thesis, California Institute of Technology (2015).
- [18] D. V. Martynov, E. D. Hall, B. P. Abbott, R. Abbott, T. D. Abbott, C. Adams, R. X. Adhikari, R. A. Anderson, S. B. Anderson, K. Arai, and et al., *Phys. Rev. D* **93**, 112004 (2016), arXiv:1604.00439 [astro-ph.IM].
- [19] E. D. Hall, *Long-Baseline Laser Interferometry for the Detection of Binary Black-Hole Mergers*, Ph.D. thesis, California Institute of Technology (2017).
- [20] B. P. Abbott, R. Abbott, T. D. Abbott, F. Acernese, K. Ackley, C. Adams, T. Adams, P. Addesso, R. X. Adhikari, V. B. Adya, and others. (LIGO Scientific Collaboration and Virgo Collaboration), *Phys. Rev. Lett.* **119**, 161101 (2017).
- [21] L. Barsotti, M. Evans, and P. Fritschel, *Classical and Quantum Gravity* **27**, 084026 (2010).
- [22] F. Matichard, B. Lantz, R. Mittleman, K. Mason, J. Kissel, B. Abbott, S. Biscans, J. McIver, R. Abbott, S. Abbott, E. Allwine, S. Barnum, J. Birch, C. Celerier, D. Clark, D. Coyne, D. DeBra, R. DeRosa, M. Evans, S. Foley, P. Fritschel, J. A. Giaime, C. Gray, G. Grabeel, J. Hanson, C. Hardham, M. Hillard, W. Hua, C. Kucharczyk, M. Landry, A. L. Roux, V. Lhuillier, D. Macleod, M. Macinnis, R. Mitchell, B. O'Reilly, D. Ottaway, H. Paris, A. Pele, M. Puma, H. Radkins, C. Ramet, M. Robinson, L. Ruet, P. Sarin, D. Shoemaker, A. Stein, J. Thomas, M. Vargas, K. Venkateswara, J. Warner, and S. Wen, *Classical and Quantum Gravity* **32**, 185003 (2015).
- [23] F. Matichard, B. Lantz, K. Mason, R. Mittleman, B. Abbott, S. Abbott, E. Allwine, S. Barnum, J. Birch, S. Biscans, D. Clark, D. Coyne, D. DeBra, R. DeRosa, S. Foley, P. Fritschel, J. Giaime, C. Gray, G. Grabeel, J. Hanson, M. Hillard, J. Kissel, C. Kucharczyk, A. L. Roux, V. Lhuillier, M. Macinnis, B. O'Reilly, D. Ottaway, H. Paris, M. Puma, H. Radkins, C. Ramet, M. Robinson, L. Ruet, P. Sareen, D. Shoemaker, A. Stein, J. Thomas, M. Vargas, and J. Warner, *Precision Engineering* **40**, 273 (2015).
- [24] F. Matichard, B. Lantz, K. Mason, R. Mittleman, B. Abbott, S. Abbott, E. Allwine, S. Barnum, J. Birch, S. Biscans, D. Clark, D. Coyne, D. DeBra, R. DeRosa, S. Foley, P. Fritschel, J. Giaime, C. Gray, G. Grabeel, J. Hanson, M. Hillard, J. Kissel, C. Kucharczyk, A. L. Roux, V. Lhuillier, M. Macinnis, B. O'Reilly, D. Ottaway, H. Paris, M. Puma, H. Radkins, C. Ramet, M. Robinson, L. Ruet, P. Sareen, D. Shoemaker, A. Stein, J. Thomas, M. Vargas, and J. Warner, *Precision Engineering* **40**, 287 (2015).
- [25] B. Lantz, R. Schofield, B. O. Reilly, D. E. Clark, and D. DeBra, *Bull. Seismol. Soc. Am.* **99**, 980 (2009).
- [26] F. Matichard and M. Evans, *The Bulletin of the Seismological Society of America* **105**, 497 (2015).
- [27] F. Matichard, M. Evans, R. Mittleman, M. MacInnis, S. Biscans, K. L. Dooley, H. Sohler, A. Lauriero, H. Paris, J. Koch, P. Knothe, A. Carbajo, and C. Dufort, *Review of Scientific Instruments* **87**, 065002 (2016), <http://dx.doi.org/10.1063/1.4953110>.
- [28] K. Venkateswara, C. A. Hagedorn, M. D. Turner, T. Arp, and J. H. Gundlach, *Rev. Sci. Instrum.* **85**, 015005 (2014), arXiv:1401.4412 [physics.ins-det].
- [29] K. Venkateswara, C. Hagedorn, J. H. Gundlach, J. Kissel, J. Warner, H. Radkins, T. Shaffer, B. Lantz, R. Mittleman, F. Matichard, and R. Schofield, *Bulletin of the Seismological Society of America*, *Bulletin of the Seismological Society of America* **107** (2017).
- [30] C. M. Mow-Lowry and D. Martynov, In prep. (2018).
- [31] A. V. Cumming, A. S. Bell, L. Barsotti, M. A. Barton, G. Cagnoli, D. Cook, L. Cunningham, M. Evans, G. D. Hammond, G. M. Harry, A. Heptonstall, J. Hough, R. Jones, R. Kumar, R. Mittleman, N. A. Robertson, S. Rowan, B. Shapiro, K. A. Strain, K. Tokmakov, C. Torrie, and A. A. van Veggel, *Classical and Quantum Gravity* **29**, 035003 (2012).
- [32] J. A. Sidles and D. Sigg, *Physics Letters A* **354**, 167 (2006).
- [33] K. L. Dooley, L. Barsotti, R. X. Adhikari, M. Evans, T. T. Fricke, P. Fritschel, V. Frolov, K. Kawabe, and N. Smith-Lefebvre, *Journal of the Optical Society of America A* **30**, 2618 (2013), arXiv:1310.3662 [physics.ins-det].
- [34] P. Fritschel, M. Evans, and V. Frolov, *Optics Express* **22**, 4224 (2014).
- [35] K. Izumi and D. Sigg, *Classical and Quantum Gravity* **34**, 015001 (2017).
- [36] T. T. Fricke, N. D. Smith-Lefebvre, R. Abbott, R. Adhikari, K. L. Dooley, M. Evans, P. Fritschel, V. V. Frolov,

- K. Kawabe, J. S. Kissel, B. J. J. Slagmolen, and S. J. Waldman, *Classical and Quantum Gravity* **29**, 065005 (2012), arXiv:1110.2815 [physics.ins-det].
- [37] L. Carbone, S. M. Aston, R. M. Cutler, A. Freise, J. Greenhalgh, J. Heefner, D. Hoyland, N. A. Lockerbie, D. Lodhia, N. A. Robertson, C. C. Speake, K. A. Strain, and A. Vecchio, *Classical and Quantum Gravity* **29**, 115005 (2012).
- [38] B. N. Shapiro, R. Adhikari, J. Driggers, J. Kissel, B. Lantz, J. Rollins, and K. Youcef-Toumi, *Classical and Quantum Gravity* **32**, 015004 (2015).
- [39] S. Aston, *Optical Read-out Techniques for the Control of Test-masses in Gravitational Wave Observatories*, Ph.D. thesis, University of Birmingham (2011).
- [40] S. Hild, B. Barr, A. Bell, C. Bell, C. Bond, D. Brown, F. Bruckners, L. Carbone, and et al., *LIGO 3 Strawman Design, Team Red*, LIGO (2012), LIGO Document T1200046.
- [41] A. Buonanno and Y. Chen, *Phys. Rev. D* **64**, 042006 (2001).
- [42] H. Miao, *Exploring Macroscopic Quantum Mechanics in Optomechanical Devices*, Springer Theses (Springer Berlin Heidelberg, 2012).
- [43] D. V. Martynov, V. V. Frolov, S. Kandhasamy, K. Izumi, H. Miao, N. Mavalvala, E. D. Hall, R. Lanza, and LSC Instrument Authors, *Phys. Rev. A* **95**, 043831 (2017), arXiv:1702.03329 [physics.optics].
- [44] J. Mizuno, K. A. Strain, P. G. Nelson, J. M. Chen, R. Schilling, A. Rüdiger, W. Winkler, and K. Danzmann, *Physics Letters A* **175**, 273 (1993).
- [45] D. McClelland, N. Mavalvala, Y. Chen, and R. Schnabel, *Laser and Photonics Reviews* **5**, 677 (2011).
- [46] Ligo Scientific Collaboration, J. Abadie, B. P. Abbott, R. Abbott, T. D. Abbott, M. Abernathy, C. Adams, R. Adhikari, C. Affeldt, B. Allen, and et al., *Nature Physics* **7**, 962 (2011), arXiv:1109.2295 [quant-ph].
- [47] J. Aasi, J. Abadie, B. P. Abbott, R. Abbott, T. D. Abbott, M. R. Abernathy, C. Adams, T. Adams, P. Addesso, R. X. Adhikari, and et al., *Nature Photonics* **7**, 613 (2013), arXiv:1310.0383 [quant-ph].
- [48] H. J. Kimble, Y. Levin, A. B. Matsko, K. S. Thorne, and S. P. Vyatchanin, *Phys. Rev. D* **65**, 022002 (2001).
- [49] J. Harms, Y. Chen, S. Chelkowski, A. Franzen, H. Vahlbruch, K. Danzmann, and R. Schnabel, *Phys. Rev. D* **68**, 042001 (2003).
- [50] P. Kwee, J. Miller, T. Isogai, L. Barsotti, and M. Evans, *Phys. Rev. D* **90**, 062006 (2014).
- [51] P. R. Saulson, *Phys. Rev. D* **42**, 2437 (1990).
- [52] G. González, *Classical and Quantum Gravity* **17**, 4409 (2000), gr-qc/0006053.
- [53] G. D. Hammond, A. V. Cumming, J. Hough, R. Kumar, K. Tokmakov, S. Reid, and S. Rowan, *Classical and Quantum Gravity* **29**, 124009 (2012).
- [54] W. C. Young and R. G. Budynas, *Roark's formulas for stress and strain*, Vol. 7 (McGraw-Hill New York, 2002).
- [55] V. Mitrofanov and K. Tokmakov, *Physics Letters A* **308**, 212 (2003).
- [56] Y. Levin, *Phys. Rev. D* **57**, 659 (1998), gr-qc/9707013.
- [57] T. Hong, H. Yang, E. K. Gustafson, R. X. Adhikari, and Y. Chen, *Phys. Rev. D* **87**, 082001 (2013).
- [58] W. Yam, S. Gras, and M. Evans, *Phys. Rev. D* **91**, 042002 (2015).
- [59] S. Gras, H. Yu, W. Yam, D. Martynov, and M. Evans, *Phys. Rev. D* **95**, 022001 (2017), arXiv:1609.05595 [physics.ins-det].
- [60] J. Steinlechner, I. W. Martin, R. Bassiri, A. Bell, M. M. Fejer, J. Hough, A. Markosyan, R. K. Route, S. Rowan, and Z. Tornasi, *Phys. Rev. D* **93**, 062005 (2016).
- [61] P. R. Saulson, *Phys. Rev. D* **30**, 732 (1984).
- [62] J. C. Driggers, J. Harms, and R. X. Adhikari, *Phys. Rev. D* **86**, 102001 (2012).
- [63] T. Creighton, *Classical and Quantum Gravity* **25**, 125011 (2008), gr-qc/0007050.
- [64] M. Coughlin, N. Mukund, J. Harms, J. Driggers, R. Adhikari, and S. Mitra, *Classical and Quantum Gravity* **33**, 244001 (2016), arXiv:1606.01716 [gr-qc].
- [65] E. Flanagan and K. Thorne, *Noise Due to Backscatter Off Baffles, the Nearby Wall, and Objects at the Fare End of the Beam Tube; and Recommended Actions*, LIGO (1994), LIGO Document T940063-x0.
- [66] D. J. Ottaway, P. Fritschel, and S. J. Waldman, *Opt. Express* **20**, 8329 (2012).
- [67] B. Canuel, E. Genin, G. Vajente, and J. Marque, *Opt. Express* **21**, 10546 (2013).
- [68] H.-Y. Chen, D. E. Holz, J. Miller, M. Evans, S. Vitale, and J. Creighton, *ArXiv e-prints* (2017), arXiv:1709.08079.
- [69] A. Sesana, J. Gair, I. Mandel, and A. Vecchio, *ApJ* **698**, L129 (2009), arXiv:0903.4177 [astro-ph.CO].
- [70] T. Damour, B. R. Iyer, and B. S. Sathyaprakash, *Phys. Rev. D* **62**, 084036 (2000), gr-qc/0001023.
- [71] M. Hannam, P. Schmidt, A. Bohé, L. Haegel, S. Husa, F. Ohme, G. Pratten, and M. Pürrer, *Phys. Rev. Lett.* **113**, 151101 (2014).
- [72] P. Ajith, M. Hannam, S. Husa, Y. Chen, B. Brügmann, N. Dorband, D. Müller, F. Ohme, D. Pollney, C. Reisswig, L. Santamaría, and J. Seiler, *Phys. Rev. Lett.* **106**, 241101 (2011).
- [73] L. Santamaría, F. Ohme, P. Ajith, B. Brügmann, N. Dorband, M. Hannam, S. Husa, P. Mösta, D. Pollney, C. Reisswig, E. L. Robinson, J. Seiler, and B. Krishnan, *Phys. Rev. D* **82**, 064016 (2010), arXiv:1005.3306 [gr-qc].
- [74] P. Schmidt, F. Ohme, and M. Hannam, *Phys. Rev. D* **91**, 024043 (2015), arXiv:1408.1810 [gr-qc].
- [75] K. Somiya, *Classical and Quantum Gravity* **29**, 124007 (2012), arXiv:1111.7185 [gr-qc].
- [76] J. Veitch, V. Raymond, B. Farr, W. Farr, P. Graff, S. Vitale, B. Aylott, K. Blackburn, N. Christensen, M. Coughlin, W. Del Pozzo, F. Feroz, J. Gair, C.-J. Haster, V. Kalogera, T. Littenberg, I. Mandel, R. O'Shaughnessy, M. Pitkin, C. Rodriguez, C. Röver, T. Sidery, R. Smith, M. Van Der Sluys, A. Vecchio, W. Vousden, and L. Wade, *Phys. Rev. D* **91**, 042003 (2015).
- [77] C. L. Rodriguez, M. Zevin, C. Pankow, V. Kalogera, and F. A. Rasio, *ApJ* **832**, L2 (2016), arXiv:1609.05916 [astro-ph.HE].
- [78] E. D. Kovetz, *Phys. Rev. Lett.* **119**, 131301 (2017).
- [79] B. P. Abbott, R. Abbott, T. D. Abbott, M. R. Abernathy, F. Acernese, K. Ackley, C. Adams, T. Adams, P. Addesso, R. X. Adhikari, and et al., *Physical Review X* **6**, 041015 (2016), arXiv:1606.04856 [gr-qc].
- [80] K. Belczynski, T. Bulik, C. L. Fryer, A. Ruitter, F. Valsecchi, J. S. Vink, and J. R. Hurley, *ApJ* **714**, 1217 (2010), arXiv:0904.2784 [astro-ph.SR].
- [81] C. L. Rodriguez, S. Chatterjee, and F. A. Rasio, *Phys. Rev. D* **93**, 084029 (2016), arXiv:1602.02444 [astro-

- ph.HE].
- [82] S. Bird, I. Cholis, J. B. Muñoz, Y. Ali-Haïmoud, M. Kamionkowski, E. D. Kovetz, A. Raccanelli, and A. G. Riess, *Phys. Rev. Lett.* **116**, 201301 (2016).
- [83] D. Christodoulou, *Phys. Rev. Lett.* **67**, 1486 (1991).
- [84] É. É. Flanagan and É. Racine, *Phys. Rev. D* **75**, 044001 (2007), gr-qc/0601029.
- [85] M. Favata, *ApJ* **696**, L159 (2009), arXiv:0902.3660 [astro-ph.SR].
- [86] P. D. Lasky, E. Thrane, Y. Levin, J. Blackman, and Y. Chen, *Physical Review Letters* **117**, 061102 (2016), arXiv:1605.01415 [astro-ph.HE].
- [87] H. Yu and N. N. Weinberg, *MNRAS* **470**, 350 (2017), arXiv:1705.04700 [astro-ph.HE].
- [88] N. Andersson and W. C. G. Ho, *ArXiv e-prints* (2017), arXiv:1710.05950 [astro-ph.HE].

Supplemental Material for “Prospects for detecting gravitational waves at 5 Hz with ground-based detectors”

(Dated: December 18, 2017)

I. LIGO-LF SUSPENSION DESIGN

LIGO-LF adopts a 4-stage suspension system similar to that of aLIGO [1]. The suspension chain consists of a top mass (TOP), an upper-intermediate mass (UIM), a penultimate mass (PUM), and a main test mass (TST), with the parameters for each stage summarized in TABLE I. The blade design used for LIGO-LF vertical support is similar to that of aLIGO. Two requirements are set for the system above 5 Hz: the suspension needs to provide sufficient filtering of the residual ground motion (cf. FIG. 2 of the main Letter), and its total thermal noise should be dominated by the pendulum mode from the TST stage.

To achieve the seismic isolation requirement, the mass ratio between the TOP and the TST stages should be similar to that of aLIGO. Decreasing the TOP mass shifts the highest suspension resonance to higher frequencies, making the pendulum filtering less efficient at 5 Hz. Consequently we choose $m_{\text{TOP}} = m_{\text{UIM}} = 80$ kg, and the resultant seismic noise is shown in the dotted-brown curve of FIG. 1 of the main Letter.

In addition to the direct length coupling, the longitudinal ground motion can also couple to the pitch motion of the test mass. The main pitch resonance frequency can be controlled by tuning the distance between the fiber binding point and the mirror’s center of mass. Similarly, the ground rotation can couple to the yaw motion of the test mass, and the resonance frequency can be controlled as well [2]. For LIGO-LF, the main pitch and yaw resonances are set to 0.42 Hz and 0.35 Hz, respectively, to balance the requirements for more filtering at high frequency (> 5 Hz) and for less rms angular motions at low frequency (< 1 Hz).

We present the suspension thermal noise for LIGO-LF in FIG. 1. In the sensitivity band above 5 Hz, the dominant contribution comes from the pendulum mode of the test mass stage. In the calculation we have assumed an effective loss angle of 5×10^{-10} [3] and the resultant suspension thermal noise is similar to the quantum noise from 5 to 20 Hz. In order to reduce the contamination from other stages, we replace the suspension for the PUM stage from C70 steel wire to silica fiber. Meanwhile, the wire stress in the TOP and UIM stages is increased by 30% relative to aLIGO for better dilution of the losses.

Besides the thermal motion along the beam line, the vertical vibration of the test masses also couples to the GW channel due to the Earth’s radius of curvature. The eigenfrequency f_v of the last stage’s vertical mode (also known as the “bounce mode”) scales as [4]

$$2\pi f_v \approx \sqrt{\frac{gY}{l\sigma} \frac{m_{\text{TST}} + m_{\text{PUM}}}{m_{\text{PUM}}}}, \quad (1)$$

where g , Y , l , σ , m_{TST} , and m_{PUM} are the local gravitational acceleration, the Young’s modulus of the material, the length of the suspension, the stress inside the fiber, the mass of the test mass, and the mass of the penultimate mass, respectively. To make f_v low, we maintain the mass ratio between the PUM and the test mass to 1 as aLIGO, and double l to 1.2 m. Meanwhile, the fibers suspending the test mass have a tapered geometry: for the thick part where most of the bending energy is stored, it has a diameter of $1.8 \mu\text{m}$ to cancel the thermal-elastic noise, while the thin part has a diameter of $0.6 \mu\text{m}$ to increase the stress σ to 1.7 GPa. Consequently, the bounce mode has an eigenfrequency of $f_v = 4.3$ Hz, which provides sufficient filtering of the vertical motion in the sensitivity band.

Lastly, we point out as a caveat that the suspension system we propose here will result in a payload close to the limit of the capacity of the current vacuum chamber piers. The implementation of it will thus require the masses to be carefully centered in the chamber so that the capacity can be fully utilized. On the other hand, decreasing the TOP/UIM masses will degrade the seismic isolation performance, while decreasing the PUM mass will increase the

TABLE I. Summary of the LIGO-LF suspension parameters

Stage	mass [kg]	length [m]	Wire diameter [mm]	Material
TOP	80	0.32	1.8	C70 steel
UIM	80	0.32	1.2	C70 steel
PUM	200	0.36	1.2	Silica
TST	200	1.2	0.6 (thin); 1.8 (thick)	Silica

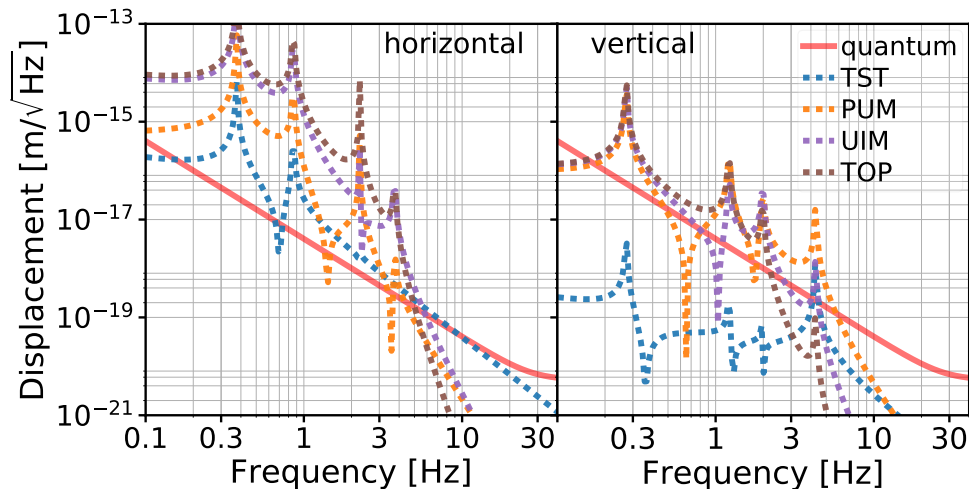


FIG. 1. The LIGO-LF suspension thermal noise from different stages (represented by dotted lines with different colors). The quantum noise is also plotted in the red-solid line as a reference. In the left we plot the direct horizontal (along the beam line) displacement noises. The dominant contribution above 5 Hz is from the last stage and it is similar to the quantum noise in the 5 – 20 Hz band. In the right are the noises due to the vertical-to-horizontal coupling. The bounce mode is at 4.3 Hz, making the vertical contributions subdominant above 5 Hz.

vertical thermal noise. This illustrates an example of the challenges that need to be tackled in order to observe GW down to 5 Hz.

II. REQUIREMENTS OF THE ANGULAR CONTROL LOOP

The alignment loop of the arm cavity is designed to balance two requirements. On one hand, the loop needs to have large enough gain at low frequency to suppress the rms motion of the test mass to $\simeq 1$ nrad, and to overcome a radiation pressure induced angular instability. On the other hand, the loop gain needs to be as low as possible at high frequency to avoid perturbing the mirrors by feeding back the sensing noise.

In FIG. 2 we plot the residual pitch motion for aLIGO and LIGO-LF after the alignment control is engaged with a detailed noise budget; the yaw motion is similar at high frequencies and is significantly less than pitch below 1 Hz, so the low frequency rms requirement for yaw is less critical. In the calculation for aLIGO, we use the measured ground motion and shadow sensor noise to represent the contributions due to seismic and due to suspension damping, respectively. For LIGO-LF, we adopt the required sensor noise (the black trace in FIG. 2 of the main Letter) for the residual seismic motion, and scale the shadow sensor noise of aLIGO down by a factor of 100 for the damping noise. Therefore our results here should be interpreted as the requirement set for the future seismic and damping sensors. The sensing noise from the wave-front sensors is assumed to be 5×10^{-15} rad/ $\sqrt{\text{Hz}}$ for both aLIGO and LIGO-LF. Also shown in the red curve as a comparison is the equivalent quantum noise: with 1 mm of spot miscentering, an angular fluctuation per test mass given by the red curve will be converted to a length noise equal to the LIGO-LF's quantum limit.

For aLIGO, a control bandwidth of 3 Hz is necessary to reduce the rms pitch motion to 1.2 nrad. Such a high bandwidth limits how fast the loop gain can roll-off at high frequency. Consequently, a considerable amount of control noise is injected to the 10-20 Hz band, contaminating the GW sensitivity. For LIGO-LF, however, we can reduce the bandwidth to 0.8 Hz, yielding a rms motion of 0.5 nrad. We require the rms motion to be less than half of the aLIGO's value to open up the possibility of increasing the spot size by 50%. The sensing noise can now be decreased below the quantum limit at 4 Hz. The damping noise, nonetheless, becomes significant for LIGO-LF, and a factor of 100 improvement is essential for reaching the instrument's fundamental limit at 5 Hz.

In addition to suppressing the test masses' rms motion, overcoming the angular instability is another critical requirement on the alignment bandwidth. With 0.8 MW of power circulating in the arms, the radiation pressure force creates an optical torque comparable to the restoring torque from the suspension, and thus modifies the test masses' mechanical response. The input and end test masses are coupled by this effect to oscillate in a set of eigenmodes

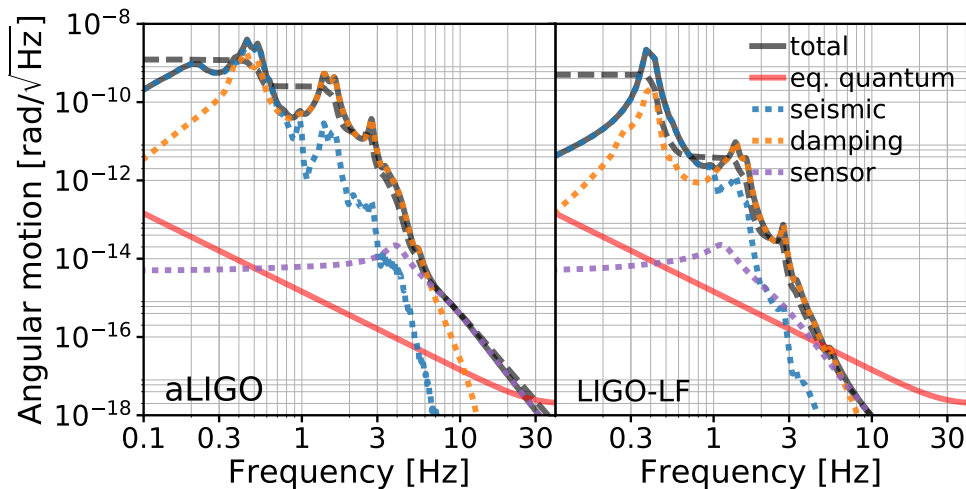


FIG. 2. The residual pitch motion of aLIGO (left panel) and LIGO-LF (right panel). The black-solid curves are the total angular motion and the black-dashed ones are the corresponding cumulative rms values. The dotted curves are the noise contributions due to seismic (blue), suspension damping (orange), and wave-front sensing (purple), respectively. The red-solid curve is shown for comparison: it corresponds to a noise level equivalent to the LIGO-LF’s quantum noise if the spot miscentering is 1 mm.

which are conventionally known as the “hard” and the “soft” modes [5]. Their eigenfrequencies are given by [6].

$$\omega_{\pm}^2 = \omega_0^2 + \frac{PL}{Ic} \left[\frac{-(g_i + g_e) \pm \sqrt{4 + (g_i - g_e)^2}}{1 - g_i g_e} \right], \quad (2)$$

where we have used ω_+ (ω_-) to represent the angular eigenfrequency of the hard (soft) mode, and ω_0 the pendulum frequency. The L , P , I , and $g_{i(e)}$ are the arm length, power circulating in the arms, momentum of inertia, and the g parameter of the input (end) test mass, respectively. The values for aLIGO are given in REF. [7], which leads to $(\omega_-/2\pi)^2 = -(0.2 \text{ Hz})^2$. The soft mode is thus unstable for aLIGO without control loop. Overcoming the instability will demand a bandwidth of $\gtrsim 10 |\omega_-/2\pi| = 2 \text{ Hz}$. Nevertheless, as we increase the test masses by a factor of 5 to 200 kg, the momentum of inertia will increase by a factor of $5^{5/3} \simeq 15$ if we assume the mirror geometry stays the same as that of the aLIGO mirror. This increased momentum of inertia greatly suppresses the radiation pressure effect. Also taking into account the facts that we shift the pendulum frequencies for LIGO-LF (cf. Section I) and modified the input test masses’ radius of curvature to increase the spot size ($g_i = -1.2$ for LIGO-LF; g_e is the same for LIGO-LF and aLIGO), the eigenfrequency of LIGO-LF’s pitch (yaw) soft mode becomes $(\omega_-/2\pi) \simeq 0.4 \text{ Hz}$ (0.3 Hz). Consequently, the soft mode will be stable for LIGO-LF, relaxing requirements set on the minimum control bandwidth.

III. CALCULATION OF THE SCATTERING NOISE

For the scattering noise calculation, we introduce the effective displacement \bar{x}_{scatter} defined as

$$\bar{x}_{\text{scatter}}(t) = \frac{\lambda}{4\pi} \sin \left[\frac{4\pi}{\lambda} x_{\text{scatter}}(t) \right], \quad (3)$$

where $x_{\text{scatter}}(t)$ is the (physical) relative displacement between a mirror and a scattering surface at time t , and $\lambda = 1064 \text{ nm}$ the laser wavelength. The corresponding frequency-domain displacement is thus given by

$$\hat{x}_{\text{scatter}}(f) = \frac{\lambda}{4\pi} \int \sin \left[\frac{4\pi}{\lambda} x_{\text{scatter}}(t) \right] \exp(-2\pi i f t) dt. \quad (4)$$

Notice that when $x_{\text{scatter}} \sim \lambda$, the effective displacement no more varies linearly with the physical displacement. Consequently, the large ground motion below 1 Hz can be up-converted to the sensitivity band, making scattering a significant noise source when the ground motion is severe.

The olive trace in FIG. 1 of the main Letter is calculated including two effects: scattering in the arm tubes, and scattering in the vertex of the interferometer, with each one’s contribution individually shown in FIG. 3.

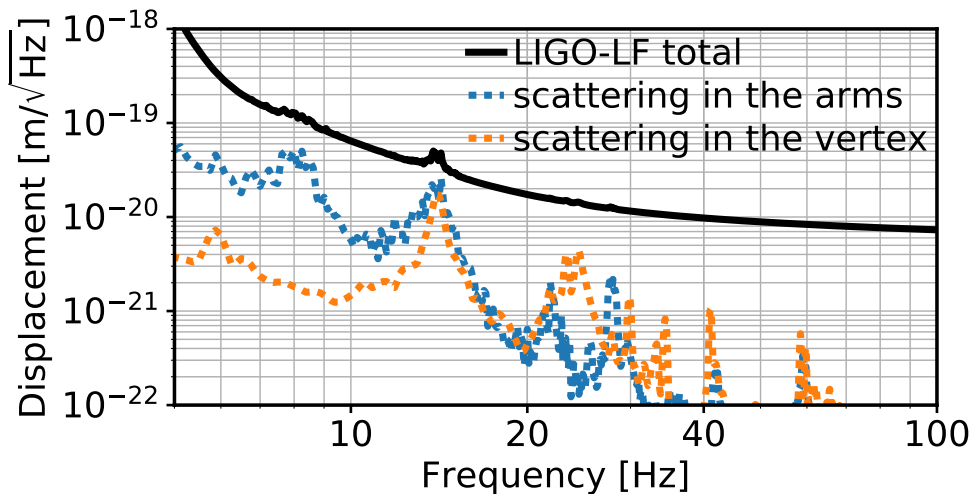


FIG. 3. The noises due to scattering in the arm tubes (dotted-blue) and in the vertex (dotted-orange). The total LIGO-LF noise is shown in the solid-black as a reference.

For the former, the calculation follows from REF. [8], and the noise projected onto the GW readout is the product between $\hat{x}_{\text{scatter}}(f)$ and the coefficient Z_{scatter} we have introduced in Eq. (1) of the main Letter.

The scattering in the vertex is caused by the anti-reflecting (AR) surfaces along the optical path. If not properly baffled, the stray light may hit the chamber wall and be reflected back to the optical path. The coupling coefficient per stray beam is [9]

$$Z_{\text{vertex}} \simeq 1.0 \times 10^{-12} \left(\frac{R_{\text{AR}}}{250 \text{ ppm}} \right) \left(\frac{2 \text{ mm}}{w_{\text{wall}}} \right) \left(\frac{T_{\text{baffle}}}{0.001} \right)^{1/2} \frac{\text{m}}{\text{m}}, \quad (5)$$

where R_{AR} is the power reflectivity of the AR surface creating the beam, w_{wall} is the stray light's spot size on the chamber wall, and T_{baffle} is the fraction (in power) of the stray light that leaks through the baffle. There are 10 AR surfaces that can contribute to this noise, 2 from the input test masses ($R_{\text{AR}} \simeq 250 \text{ ppm}$), 4 from the beam splitter ($R_{\text{AR}} \simeq 50 \text{ ppm}$), and 4 from the compensation plates ($R_{\text{AR}} \simeq 20 \text{ ppm}$). To achieve the proposed LIGO-LF sensitivity, the baffles need to reduce the power of the stray light by

$$T_{\text{baffle}}^{(\text{LIGO-LF req.})} < 0.1\%. \quad (6)$$

IV. INFERRED MASSES IN THE SOURCE-FRAME

In the main Letter, the parameter estimation section focused on the results in the detector-frame. Here we provide the source-frame results for completeness. The conversion is [10]

$$\mathcal{M}_c = \frac{\mathcal{M}_c^{(d)}}{1+z} \quad (7)$$

for the chirp mass \mathcal{M}_c , and similarly for the total mass M_{tot} . Here z is the cosmological redshift and we have denoted the detector-frame with a superscript (d).

In FIG. 4 we present the 90% credible intervals of the redshift z . To yield a network SNR of 16 with aLIGO design sensitivity, the redshifts are $z = (0.53, 0.82, 1.1, 0.92, 0.22)$ for the 5 injections we have with $M_{\text{tot}}^{(d)} = (100, 200, 400, 1000, 2000) M_{\odot}$, respectively. LIGO-LF typically improves the accuracy in the redshift inference by a factor of 2 relative to aLIGO.

We show the 90% credible intervals of the source-frame masses in FIG. 5. The injected source-frame total masses are $M_{\text{tot}} = (65, 109, 187, 521, 1644) M_{\odot}$, and chirp masses $\mathcal{M}_c = (28, 48, 82, 227, 716) M_{\odot}$. Due to the statistical error in measuring the redshift, LIGO-LF only constrains the source-frame values 2 times better than aLIGO, despite that it can constrain the detector-frame ones 3-5 times better.

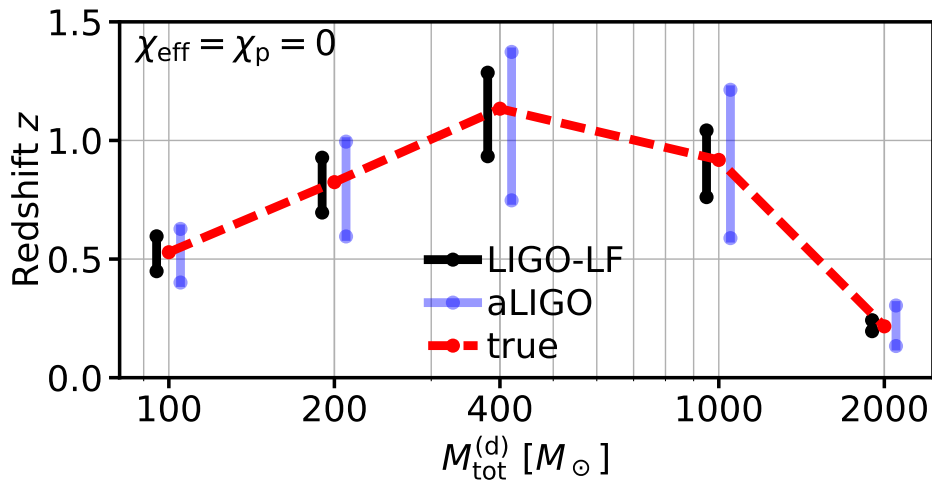


FIG. 4. Mock sources for each total mass were placed at the redshifts indicated by the red-dashed line. The redshifts were chosen to give a network SNR of 16 in aLIGO. The black (blue) bars indicate the 90% credible interval for the inferred redshift with LIGO-LF (aLIGO) sensitivity. LIGO-LF typically improves the constrain in z by a factor of 2.

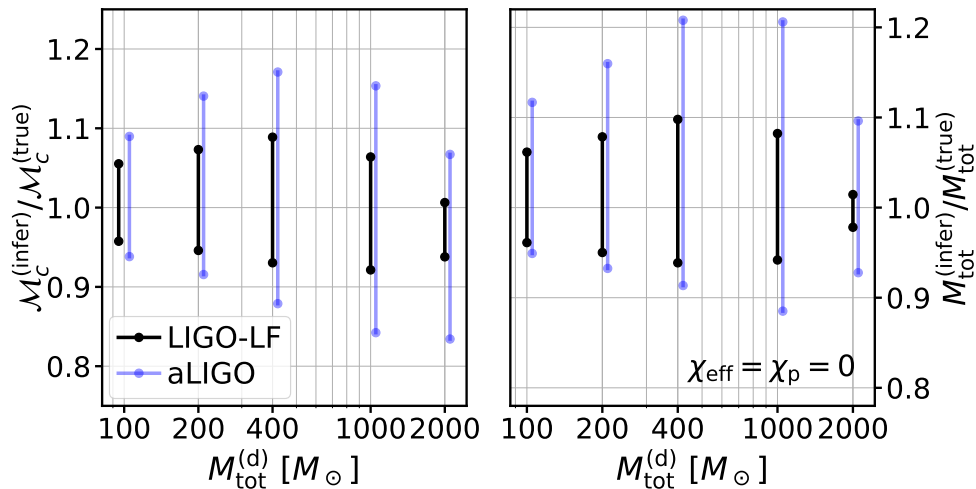


FIG. 5. The 90% credible interval of the source-frame chirp mass \mathcal{M}_c (left panel) and total mass M_{tot} (right panel). The uncertainty is about a factor of 2 smaller for LIGO-LF compared to aLIGO, and is dominated by the uncertainty in inferring the redshift. Thus LIGO-LF enables less improvement in constraining the source-frame masses than in the detector-frame ones.

-
- [1] S. M. Aston, M. A. Barton, A. S. Bell, N. Beveridge, B. Bland, A. J. Brummitt, G. Cagnoli, C. A. Cantley, L. Carbone, A. V. Cumming, L. Cunningham, R. M. Cutler, R. J. S. Greenhalgh, G. D. Hammond, K. Haughian, T. M. Hayler, A. Heptonstall, J. Heefner, D. Hoyland, J. Hough, R. Jones, J. S. Kissel, R. Kumar, N. A. Lockerbie, D. Lodhia, I. W. Martin, P. G. Murray, J. O'Dell, M. V. Plissi, S. Reid, J. Romie, N. A. Robertson, S. Rowan, B. Shapiro, C. C. Speake, K. A. Strain, K. V. Tokmakov, C. Torrie, A. A. van Veggel, A. Vecchio, and I. Wilmot, *Classical and Quantum Gravity* **29**, 235004 (2012).
- [2] M. Rakhmanov, *Dynamics of laser interferometric gravitational wave detectors*, Ph.D. thesis, CALIFORNIA INSTITUTE OF TECHNOLOGY (2000).
- [3] G. D. Hammond, A. V. Cumming, J. Hough, R. Kumar, K. Tokmakov, S. Reid, and S. Rowan, *Classical and Quantum Gravity* **29**, 124009 (2012).
- [4] P. Fritschel, D. Shoemaker, and D. Coyne, *Low-frequency Cutoff for Advanced LIGO*, LIGO (2002), LIGO Document T020034.

- [5] J. A. Sidles and D. Sigg, *Physics Letters A* **354**, 167 (2006).
- [6] E. Hirose, K. Kawabe, D. Sigg, R. Adhikari, and P. R. Saulson, *Appl. Opt.* **49**, 3474 (2010), arXiv:0909.0010 [gr-qc].
- [7] L. Barsotti, M. Evans, and P. Fritschel, *Classical and Quantum Gravity* **27**, 084026 (2010).
- [8] D. J. Ottaway, P. Fritschel, and S. J. Waldman, *Opt. Express* **20**, 8329 (2012).
- [9] D. Martynov, “Estimation of scattering noise from the ghost beams,” <https://alog.ligo-la.caltech.edu/aLOG/index.php?callRep=29665> (2016), aLIGO LLO Logbook 29665.
- [10] C. Cutler and É. E. Flanagan, *Phys. Rev. D* **49**, 2658 (1994), gr-qc/9402014.